Z. Phys. B - Condensed Matter 85, 135-143 (1991)

Condensed Matter
Zeitschrift für Physik B

Field applied (FMD) computer simulation of the frequency doubled optical Stark effect

M.W. Evans*

Institute of Physical Chemistry, University of Zürich, Winterthurerstrasse 190, CH-8057 Zürich, Switzerland

Received May 3, 1991; revised version June 4, 1991

It is shown by field applied molecular dynamics computer simulation (FMD) of liquid water that the frequency doubled optical Stark effect is accompanied by novel second order rise transients which have no known counterpart in orientational theory, based on Langevin/Kielich functions. In the statistically stationary, post transient, steady state, correlation function have been computed which are intricately dependent on the frequency of the pump laser. These transients can be obtained experimentally by modifications of optical Stark effect apparatus for measurement on a femtosecond time scale.

0. Introduction

The optical Stark effect is defined through the induction of an electric dipole moment by the following type of interaction between molecular polarisability and the electric field strength, $\underset{\sim}{E}$, of an electromagnetic plane wave

$$\mu_i^{(\mathrm{ind})} = \alpha_{ij}(-\omega;\omega)\, E_j . \tag{1}$$

We consider at the outset the electric field defined as the plus conjugate of a left circularity polarised plane wave

$$\underset{\sim}{E}_L^+ = E_0(\underset{\sim}{i} - \mathrm{i}\underset{\sim}{j})\exp(\mathrm{i}\phi_L) . \tag{2}$$

Here $\underset{\sim}{i}$ and $\underset{\sim}{j}$ are unit vectors in the X and Y axes, respectively, of the laboratory frame (X, Y, Z), and the phase factor is defined by

$$\phi_L = \omega t - \underset{\sim}{K}_L \cdot \underset{\sim}{r} \tag{3}$$

where ω is the angular frequency in radians per second of the plane wave, t the time, $\underset{\sim}{K}_L$ the left handed propagation vector, and $\underset{\sim}{r}$ a position vector. For the purposes of computer simulation, we approximate the phase by

$$\phi_L \doteq \omega t . \tag{4}$$

Usually in the treatment of the optical Stark effect [1] the potential energy and torque generated by the interaction of $\underset{\sim}{E}$ with the induced electric dipole moment $\underset{\sim}{\mu}^{(\mathrm{ind})}$ are described respectively by the time independent expression

$$\Delta H_S = -\underset{\sim}{\mu}^{(\mathrm{ind})} \cdot \underset{\sim}{E}^* \tag{5}$$

and

$$\underset{\sim}{T}_S = -\underset{\sim}{\mu}^{(\mathrm{ind})} \times \underset{\sim}{E}^* . \tag{6}$$

Here $\underset{\sim}{E}_L^{*+}$ is the complex conjugate of $\underset{\sim}{E}_L^+$, i.e.

$$\underset{\sim}{E}_L^{*+} = E_0(\underset{\sim}{i} + \mathrm{i}\underset{\sim}{j})\exp(-\mathrm{i}\phi_L) , \tag{7}$$

so that the phase factor, ϕ_L, disappears in the vector dot and cross products (5) and (6) respectively. The time (i.e. phase) independent energy term (5) can then be applied straightforwardly [2, 3] to the generation of Langevin-Kielich functions [4] which describe ensemble orientational averages of the optical Stark effect.

In this paper, we consider the thermodynamic and molecular dynamic characteristics of a torque of type

$$\underset{\sim}{T}_S^{(2\omega)} = -\underset{\sim}{\mu}^{(\mathrm{ind})} \times \underset{\sim}{E}_L^+ \tag{8}$$

in which the optical Stark effect is accompanied by second harmonic generaion. The energy corresponding to this torque is

$$\Delta H_S^{(2\omega)} = -\underset{\sim}{\mu}^{(\mathrm{ind})} \cdot \underset{\sim}{E}_L^+ \tag{9}$$

and disappears when time averaged. In consequence, the Langevin description of orientational averages produced by the torque (8) cannot be implemented [5]. Use is made in this paper therefore of field applied molecular dynamics computer simulation (FMD) to investigate the orientational thermodynamics with rise transients and time correlation functions.

* *Permanent address:* 433 Theory Center, Cornell University, Ithaca, NY 14853, USA

In Sect. 1, the torque (8) is worked out in the molecule fixed frame of water, assuming that the molecular polarisability is a pure real quantity [6] which can be diagonalised in the same frame (1, 2, 3) as the principal molecular moments of inertia of water. Section 2 develops the theory with the use of FMD in an ensemble of 108 molecules interacting with a well tested site-site potential. Section 3 presents results in terms of novel second order orientational transients of the type $\langle e_{1X}^n \rangle, \ldots, \langle e_{3Z}^n \rangle$, where e_i is a unit vector in axes 1, 2, or 3. Transients were computed in this work for a number of pump laser frequencies corresponding with the frequencies of experimentally available pump lasers such as the various Nd-YAG systems and dye lasers, operating in the visible. The post transient steady state in the presence of the pump laser is described in Sect. 3 with appropriate time correlation functions. The discussion extends the argument to possible experimental verification of the theoretical and numerical indications obtained in this work.

1. The torque

In a diamagnetic molecule such as water, the polarisability α_{ij} is usually taken to be pure real [7, 8]. This is an approximation which holds in the transparent region of the water spectrum, but near optical resonance, the quantity α_{ij} becomes complex. Adopting a pure real alpha it is convenient to work out the torque (8) in the frame (1, 2, 3) in preparation for the FMD computer simulation, which implements the torque [9–14] in the forces loop. The induced electric dipole moment (1) is then worked out as a pure real quantity by multiplying the real polarisability tensor by the real part of $\underset{\sim}{E}_L^+$, which frame (1, 2, 3) becomes

$$\begin{bmatrix} E_{L1}^+ \\ E_{L2}^+ \\ E_{L3}^+ \end{bmatrix} = \begin{bmatrix} e_{1X} & e_{1Y} & e_{1Z} \\ e_{2X} & e_{2Y} & e_{2Y} \\ e_{3X} & e_{3Y} & e_{3Z} \end{bmatrix} \begin{bmatrix} E_{LX}^+ \\ E_{LY}^+ \\ 0 \end{bmatrix}. \tag{10}$$

Here $\underset{\sim}{E}_L^+$ in frame (X, Y, Z) has been multiplied by a rotation matrix of unit vectors, and the (real) field components in frame (X, Y, Z) are

$$\left.\begin{aligned} E_{LX}^+ &= E_0 \cos \omega t \\ E_{LY}^+ &= E_0 \sin \omega t \\ E_{LZ}^+ &= 0 \end{aligned}\right\}. \tag{11}$$

The laser therefore propagates in axis Z.

Consequently, the electric field components in frame (1, 2, 3) are

$$\left.\begin{aligned} E_{L1}^+ &= e_{1X} E_{LX}^+ + e_{1Y} E_{LY}^+ \\ E_{L2}^+ &= e_{2X} E_{LX}^+ + e_{2Y} E_{LY}^+ \\ E_{L3}^+ &= e_{3X} E_{LX}^+ + e_{3Y} E_{LY}^+ \end{aligned}\right\}. \tag{12}$$

Assuming that the real molecular polarisability is diagonal in frame (1, 2, 3) the induced electric dipole moment in this frame is

$$\left.\begin{aligned} \mu_1^{(\mathrm{ind})} &= \alpha'_{11} E_{L1}^+ \\ \mu_2^{(\mathrm{ind})} &= \alpha'_{22} E_{L2}^+ \\ \mu_3^{(\mathrm{ind})} &= \alpha'_{33} E_{L3}^+ \end{aligned}\right\} \tag{13}$$

and the torque components in axes 1, 2, and 3 are

$$\left.\begin{aligned} T_{S1}^{(2\omega)} &= \alpha'_{22} E_{L2}^+ E_{L3}^+ - \alpha'_{33} E_{L3}^+ E_{L2}^+ \\ T_{S2}^{(2\omega)} &= \alpha'_{33} E_{L3}^+ E_{L1}^+ - \alpha'_{11} E_{L1}^+ E_{L3}^+ \\ T_{S3}^{(2\omega)} &= \alpha'_{11} E_{L1}^+ E_{L2}^+ - \alpha'_{22} E_{L2}^+ E_{L1}^+ \end{aligned}\right\}. \tag{14}$$

These torque components are proportional to the square of the electric field components, resulting in second harmonic generation. The torque is therefore phase dependent. It is finally back-transformed into the laboratory frame through the rotation matrix

$$\begin{bmatrix} T_{SX}^{(2\omega)} \\ T_{SY}^{(2\omega)} \\ T_{SZ}^{(2\omega)} \end{bmatrix} = \begin{bmatrix} e_{1X} & e_{2X} & e_{3X} \\ e_{1Y} & e_{2Y} & e_{3Y} \\ e_{1Z} & e_{2Z} & e_{3Z} \end{bmatrix} \begin{bmatrix} T_{S1}^{(2\omega)} \\ T_{S2}^{(2\omega)} \\ T_{S3}^{(2\omega)} \end{bmatrix} \tag{15}$$

and supplements the intermolecular torques computed in the forces loop of the algorithm Tetra [9], whose code is given in the literature [14].

Note that the torque depends on twice the frequency of the applied pump laser, and its effect is superimposed in an intricate way upon the natural, or thermal, molecular dynamics of the ensemble.

2. FMD computer simulation

The FMD computer simulation was carried out in liquid water at 293 K, 1.0 bar, with 108 water molecules, using a time step of 0.5 fs. The site-site interaction potential was

$$\phi_{ij} = \sum_{i,j} 4\varepsilon \left[\left(\frac{\sigma}{r_{ij}} \right)^{12} - \left(\frac{\sigma}{r_{ij}} \right)^{6} \right]$$

$$\varepsilon/k\,(H-H) = 21.1\ \mathrm{K}; \quad \sigma\,(H-H) = 2.25\ \text{Å};$$

$$\varepsilon/k\,(0-0) = 58.4\ \mathrm{K}; \quad \sigma\,(0-0) = 2.80\ \text{Å}; \tag{16}$$

$$q_H = 0.23\,|e|; \quad q_0 = 0.00\,|e|;$$

$$q(\text{lone pair}) = -0.23\,|e|,$$

which was developed [15] from the ST2, and which has been compared with the MCYL water potential [16] and with water data over a considerable thermodynamic range [17]. An initial FCC water lattice was melted into the liquid over about 6,000 time steps, the attainment of a liquid like condition being monitored through n order orientational averages such as

$$\langle e_{1Z} \rangle; \quad \langle e_{1Z}^2 \rangle; \quad \langle e_{2Z} \rangle; \quad \langle e_{2Z}^2 \rangle;$$

$$\langle e_{3Z} \rangle; \quad \langle e_{3Z}^2 \rangle$$

over unit vectors in axes 1, 2, and 3 of frame (1, 2, 3). In the liquid condition first and higher odd order averages of this type fluctuate around zero, and second order averages fluctuate around the value 1/3, fourth order around 1/5, sixth order around 1/7, and so on.

The torque (15) was applied in the liquid condition, and the development of rise transients monitored at odd and even order. All odd order ensemble averages remained around zero after the torque was switched on, but the same trajectories produced easily discernible even order rise transients, which are illustrated in the results Sect. 3 of this paper. The time evolution of these transients depends on the square of the applied scalar electric field strength, E_0^2, of the laser, and also on the laser frequency. They eventually reach a saturation level, after which the sample is in a statistically stationary state suitable for the computation of time correlation functions [18] by running time averaging.

The FMD simulation was carried out at four different laser frequencies corresponding with real pump lasers: 1) a Q switched carbon dioxide laser, operating in the mid infra red at about 30.0 THz (terahertz); 2) a mode locked neodymium phosphate glass laser at about 300.0 THz in the visible; 3) a mode locked rhodamine 6G dye laser at about 500.0 THz; 4) a passively mode locked CW dye laser at about 600.0 THz.

At each of these frequencies, rise transients at second order of the type

$$\langle e_{1Z}^2\rangle;\quad \langle e_{2Z}^2\rangle;\quad \langle e_{3Z}^2\rangle$$
$$\langle e_{1Y}^2\rangle;\quad \langle e_{2Y}^2\rangle;\quad \langle e_{3Y}^2\rangle$$
$$\langle e_{1X}^2\rangle;\quad \langle e_{2X}^2\rangle;\quad \langle e_{3X}^2\rangle$$

were computed as a function of E_0^2, building up a data bank which is available from the author. Some of these results are presented in Sect. 3 as plots of final level attained by the transient. It is precisely this kind of plot that would be analysed usually as a Langevin/Kielich function, but the latter is not accessible analytically because the energy (9) disappears over time, i.e. the average over many cycles of the phase of the pump laser disappears, in the same way that the t average of $\cos(\omega t)$ and $\sin(\omega t)$ disappears.

The data bank also consists of time correlation functions worked out in the post transient state, with pump laser switched on. The examples used were

$$C_{1ij}(t)=\frac{\langle J_i(t)\,J_j(0)\rangle}{\langle J_i^2\rangle^{1/2}\langle J_j^2\rangle^{1/2}} \tag{17}$$

the molecular angular momentum time correlation tensor;

$$C_{2ij}(t)=\frac{\langle e_{1i}(t)\,e_{1j}(0)\rangle}{\langle e_{1i}^2\rangle^{1/2}\langle e_{1j}^2\rangle^{1/2}} \tag{18}$$

the orientational time correlation tensor of vector e_1; and

$$C_{3ij}(t)=\frac{\langle \dot{e}_{1i}(t)\,\dot{e}_{1j}(0)\rangle}{\langle \dot{e}_{1i}^2\rangle^{1/2}\langle \dot{e}_{1j}^2\rangle^{1/2}} \tag{19}$$

the corresponding rotational velocity [18] time correlation tensor. These tensors are sub-categorised into auto correlation functions (ACF's), with $i=j=X$, Y, or Z; and cross correlation functions (CCF's) about the propagation axis, respectively $i=X$, $j=Y$ and $i=Y$, $j=X$. The running time average extended over 6,000 time steps, and ACF's and CCF's are displayed to a maximum of 400 time steps, giving "good statistics". Component ACF's and CCF's are displayed to show that the sample is anisotropic in the presence of the laser, and also to illustrate in full detail the molecular dynamical characteristics of the second harmonic of the optical Stark effect.

The details of transients and autocorrelation functions are markedly dependent on the diagonalised components α'_{11}, α'_{22}, and α'_{33} of the real part of the polarisability of the water molecule. Unfortunately, the literature is inconclusive in this respect, even to the extent of knowing the signs of the anisotropies of polarisability. We have dealt with this question elsewhere, in the context of the optical Kerr effect [19]. For example, Khanarian and Kent [20] tabulate a number of estimates, roughly half of which give a positive anisotropy and the other half a nagative anisotropy. This appears to be the state of the art for the water molecule, both experimentally and ab initio, and in this situation we have chosen to illustrate our methodology in this paper with one set of data, taken at random, from the careful experimental work [21] of Zeiss and Meath. These authors propose

$$\alpha'_{11}=9.62;\quad \alpha'_{22}=9.26;\quad \alpha'_{33}=10.01 \tag{20}$$

in atomic units. It should be noted carefully that the precise details of the time dependencies of our transients and correlation functions depend [19] on the values accepted for the three principal polarisabilities of water in frame (1, 2, 3), the frame of the principal molecular moments of inertia.

The structural properties of water in the field free equilibrium state from our model potential are given in the literature [17] in terms of atom-atom pair distribution functions. Figure 1 is a comparison of the O–H, H–H, and O–O pdf's for water in the absence and presence of a laser field at 600 THz. These were calculated over 6,000 time steps. These pdf's give an impression of the (small) structural damage that the laser does to the H bond network, and video animation [19] of the process shows that the main effect of the laser, approximately speaking, is to attempt to spin the molecules about the propagation axis, a process which occurs in competition with the background thermal dynamics. An extensive animation video of a similar process (inverse Zeeman effect [14]) is available on request from the author. Clearly, disruption of the H bonding network is inevitable as the energetic laser radiation forms a torque with the appropriate property tensor of each molecule in the ensemble. It has been shown [17] that H bonding in water can be described dynamically in terms of time correlation functions {18}, and at each applied laser frequency in this work there are characteristic changes in these functions, implying that the H bonding network is indeed disrupted, both structurally (pdf's) and dynamically (time correlation functions).

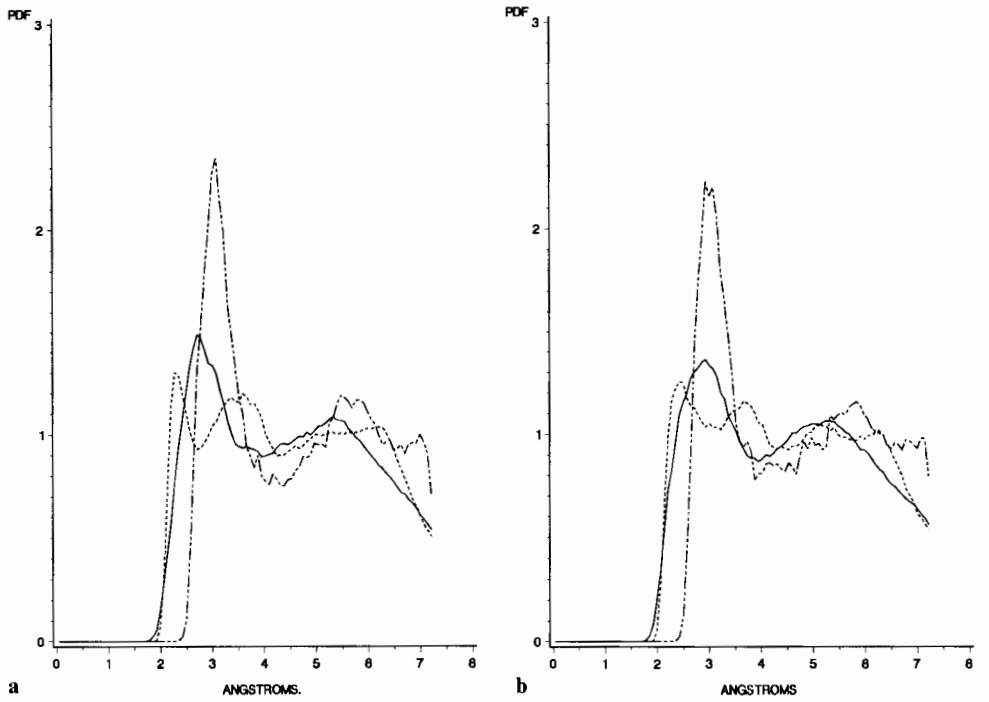

Fig. 1a, b. Atom-atom pair distribution functions for liquid water, effect of 600 THz laser in the frequency doubled optical Stark effect. —— H-H; ---- H-O; —·—·— O-O.
a Field free equilibrium;
b field applied equilibrium. The pdf's are computed over 6000 time steps of 0.1 fs in both cases, and the half box length is about 5.5 Å, Pdf's are reliable up to this cut-off point. 108 molecules were used

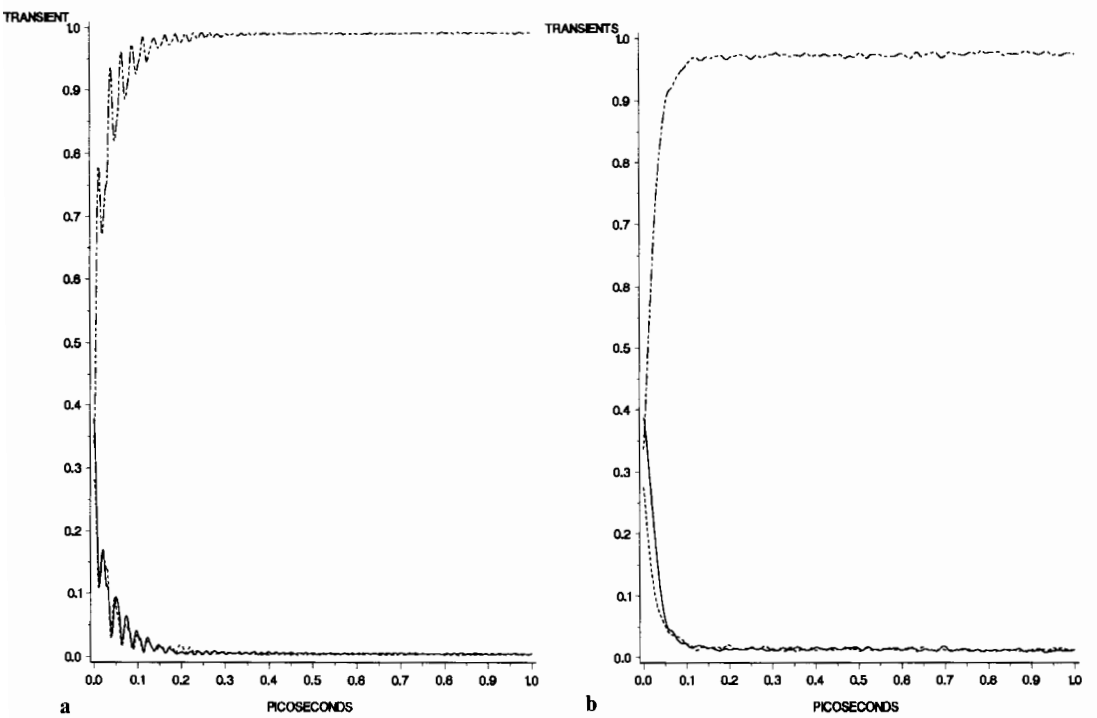

Fig. 2a, b. Second order rise transients for a 600 THz pump laser. Comparison of runs with different temperature rescaling (digital thermostatting).
a —— $\langle e_{2X}^2 \rangle$; ---- $\langle e_{2Y}^2 \rangle$; —·—·— $\langle e_{2Z}^2 \rangle$, rescaling every 50 time steps.
b As for **a**, rescaling every one time step

The energy required to do this can be measured through the increase in the configurational part of the internal potential energy computed in the FMD simulation for the ensemble. This is defined by

$$\langle U \rangle = \left\langle \sum_{i<j} \sum \phi_{ij} \right\rangle + U_C \tag{21}$$

where the sum is over all atom-atom pairs for which the interatomic distance r_{ij} is less than the cut-off distance r_C of the potential. The correction U_C is based on a uniform distribution of the molecules beyond this cut off distance r_C [14]. The configurational energy, calculated in the field-on steady state, was increased by about 20% by application of the laser.

When the laser is applied to the sample, there is an immediate increase in both rotational and translational temperature, so that there is a need for a thermostatting subroutine. This is a temperature rescaling routine [14] whose effect is to drive down the temperature every N

time steps towards the input value. Since temperature is kinetic energy, temperature rescaling means that the linear and angular velocity vectors are scaled back digitally every N time steps. Our animations show this scaling back clearly as jumps in the absolute values of the vectors, jumps which maintain the molecular trajectories of velocity or angular velocity relative to each other. The 108 linear and angular velocity vectors were animated at equilibrium and through the rise transient. At the same time, animations of the orientational vectors show that there is little or no discernible effect of temperature rescaling on the relative orientations of each molecule, i.e. there are no sudden jumps in the 108 orientation vectors as the rescaling routine is applied. This is reflected in the second order averages of Fig. 2, where there are no discontinuities. At field applied equilibrium, the re-scaling routine is maintained in action, because the laser is continuously pumping in energy to each molecule through each individual torque. We note that laser-on, steady state, time correlation functions and atom-atom pair distribution functions computed in this way show no discontinuities due to temperature rescaling.

Without this digital thermostat, the sample would heat up rapidly, the temperature would increase at each time step, and the pressure would increase, because we are using a constant volume simulation. It is highly recommended that the reader view our inverse Zeeman effect animation [14] (judged the best animation of the natural sciences category of the 1990 IBM Supercomputer Competition, and available from the author and IBM) to view directly the effect of temperature rescaling on the 108 velocity and angular velocity vectors. One animation in this context is worth a thousand words.

Digital rescaling can be applied every N time steps, and in Fig. 2 a comparison is given of the effect of rescaling every 50 time steps and every one time step for a 600 THz laser which has increased the configurational potential energy by 20%. There is little or no change in the correlation time of the rise transient, which attains the same field-on saturation level in both cases. Temperature rescaling every one time step is equivalent to maximising the efficiency of the digital thermostat, so that the kinetic energy imparted by the external field is removed at its maximum rate. The latter may be defined as a maximum temperature dissipation rate. Clearly, however, the rise transient correlation time does not depend on temperature dissipation rate to any significant degree.

Finally, on the subject of temperature rescaling, it is noteworthy that where Langevin and Langevin-Kielich functions are definable, the saturation levels of the rise transients from FMD produce the analytical Langevin functions. This was first found in 1982 using a simple static electric field [9, 10], and has recently been verified for the optical Kerr effect [25], where the interaction energy is laser phase independent and forms generalised Langevin-Kielich (GLK) functions for the asymmetric top water molecule. These GLK functions check the FMD method independently.

The model used for water is a rigid molecule approximation, and we have not considered vibrational modes, which appear at 45 and 110 THz. It would be interesting to repeat the simulation with a flexible model of water. The literature contains a comparison [16] between the present model of water and the MCYL potential, in which a detailed evaluation was made of the (small) effect of vibration on the translational and rotational molecular time correlation functions.

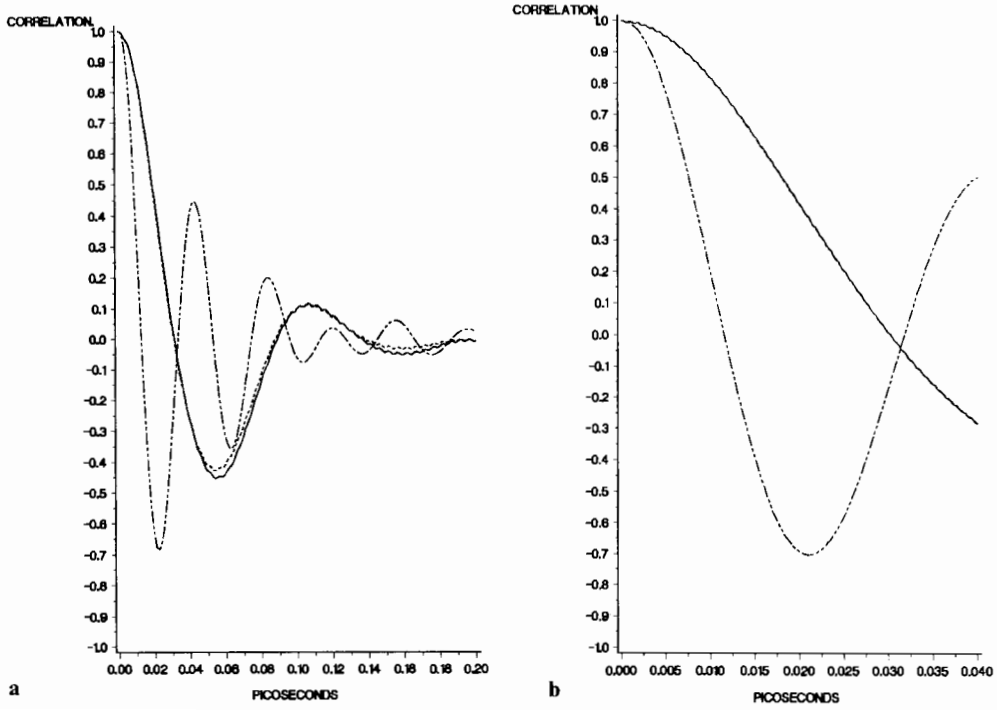

Fig. 3a, b. Comparison of rotational velocity acf's at 600 THz with different time steps. —— $i=j=X$; - - - - $i=j=Y$; — · · — · · — $i=j=Z$.
a Time step = 0.5 fs;
b Time step = 0.1 fs

Finally, the runs at 600 THz were repeated with a time step of 0.1 fs, resulting in a better resolution of the details in the rise transients and time correlation functions. A comparison of runs at 0.5 fs and 0.1 fs at this frequency is given in Fig. 3.

3. Results. Rise transients and time correlation functions

The second harmonic of the optical Stark effect is accompanied by the development of even order rise transients, an example of which is shown in Fig. 2 at 600 THz using temperature rescaling every 50 time steps and every one time step. The transients at 300 THz and 500 THz are similar in appearance to those at 600 THz. These data show that an optical pump laser at any of these three visible frequencies would generate a frequency doubled optical Stark effect which could be measured as second order orientational rise transients, i.e. birefringence would be generated on a femtosecond time scale, now accessible experimentally in, for example, the optical Kerr effect [22, 23]. This provides a new experimental method for the measurement of the anisotropy of the polarisability, while at the same time probing the molecular dynamical and diffusional [10] nature of the ensemble under investigation. It can be seen clearly in Fig. 2 that the frequency (600 THz) of the pump laser produces a well defined final level in the second order rise transients. A useful check on the FMD procedure is that the *same trajectories* produce vanishing first order averages, and there are no first order transients.

The second order transients clearly show oscillations at frequency corresponding to that of the laser. For example, at 30 THz (i.e. at the inverse of 0.033 ps. These 0.033 ps oscillations appear clearly in all nine second order transients, betraying the direct influence of the 30 THz carbon dioxide pump laser. This is a second useful check on the FMD method.

Rise transient oscillations were first derived analytically [10] and their existence later confirmed computationally [24], however, this work appears to be the first evidence for transient oscillations generated in the frequency doubled optical Stark effect by infra red and visible frequency, intense, electromagnetic pump fields of a type accessible experimentally "off the shelf" (e.g. Nd:YAG systems and carbon dioxide lasers).

When the frequency of the pump laser is reduced to zero in the FMD simulation the second order rise transients show oscillations more typical of those known already from static electric fields [24]. At zero pump frequency the role of the X and Z components of the vectors $\underset{\sim}{e}_1$, $\underset{\sim}{e}_2$ and $\underset{\sim}{e}_3$ interchange, i.e. the ordering process results in anisotropy not about the Z axis, but about the X axis. This result was produced by changing nothing in the FMD source code except the input parameter for pump laser frequency, and appears to show that ordering in the conventional (frequency independent) optical Stark effect [1] is about an orthogonal laboratory frame axis to that of the frequency doubled optical Stark effect investigated in this paper. This particular result is confirmed in the analysis of the molecular dynamical properties of the water ensemble in the post-transient state in which second order orientational averages have reached their final levels. The sequence of results for the correlation functions is discussed in order of increasing pump laser frequency. There is space here for only a few illustrations from the complete data bank, available from the author. Each set of auto-

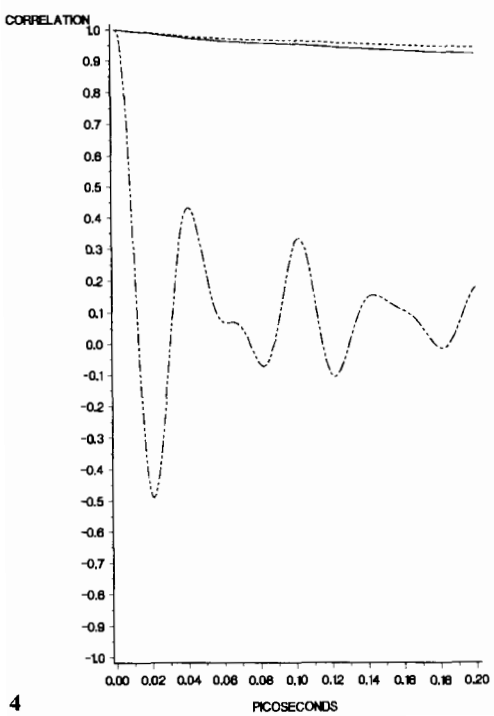

4

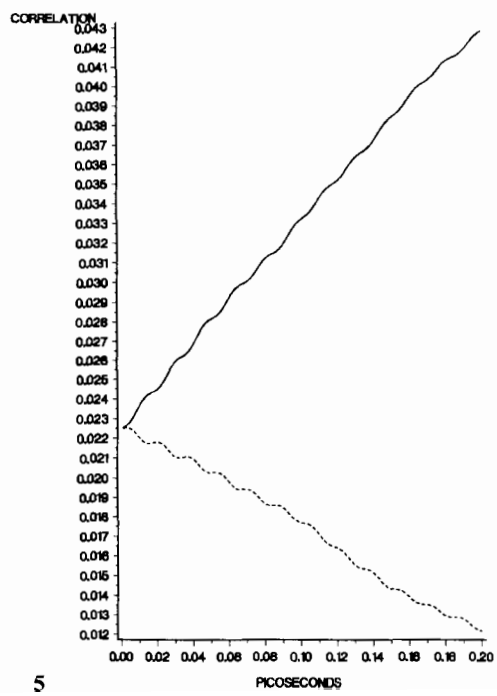

5

Fig. 4. Orientational acf's at 30 THz, 0.5 fs time step, X, Y, Z notation as for Fig. 3

Fig. 5. Orientational ccf's a 30 THz, 0.5 fs time step, —— $i=X$, $j=Y$; ---- $i=Y$, $j=X$

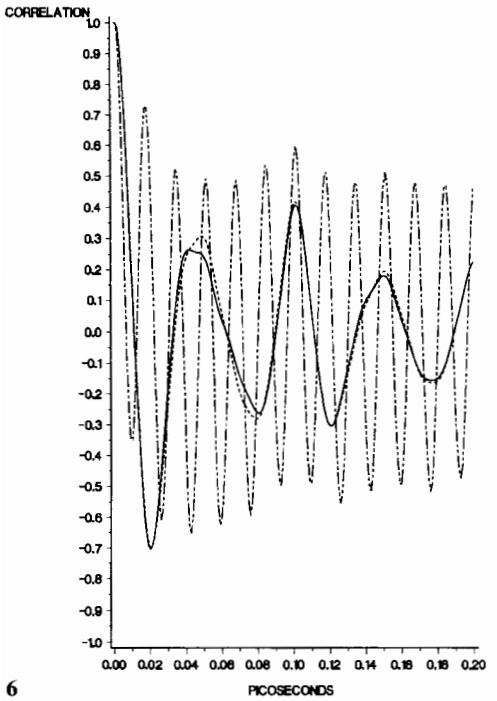

6

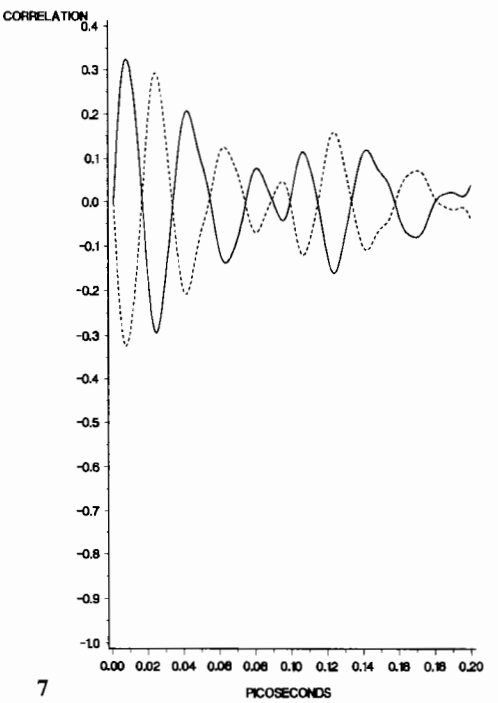

7

Fig. 6. As for Fig. 4, angular momentum acf's

Fig. 7. As for Fig. 5, angular momentum ccf's

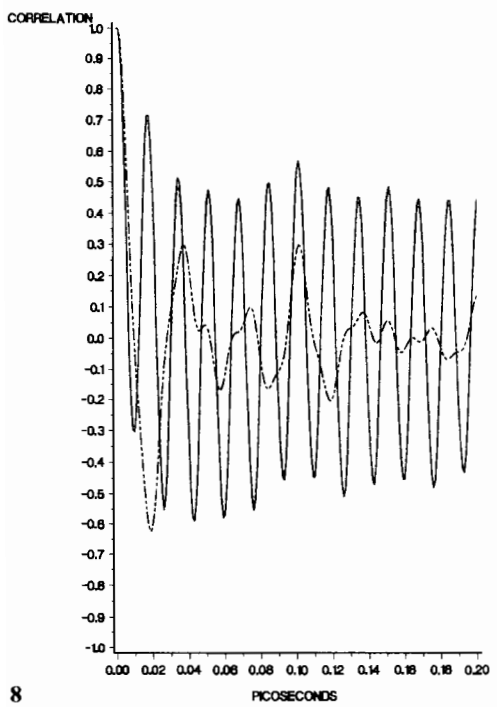

8

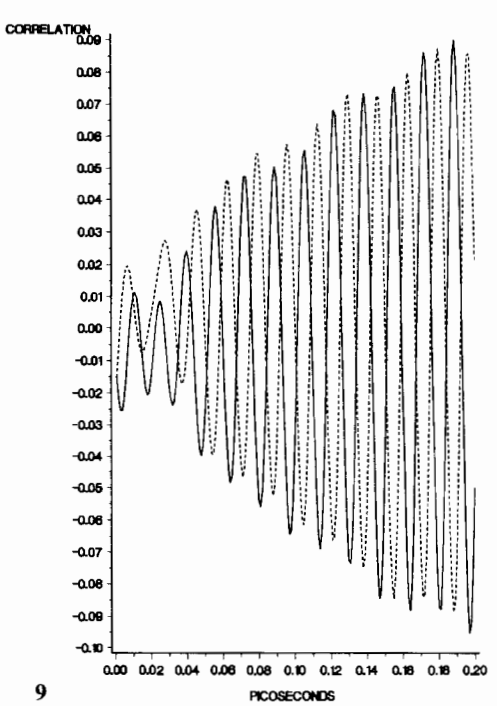

9

Fig. 8. As for Fig. 4, rotational velocity acf's

Fig. 9. As for Fig. 5, rotational velocity ccf's

correlation functions (ACF's) is followed by one of the equivalent CCF's in order to illustrate the variety of behaviour observed in this work. A complete set of time correlation functions at the 30 THz infra red pump laser frequency is illustrated in Figs. 4–9, namely: the orientational, angular momentum and rotational velocity ACF's and CCF's at this frequency. The field off equivalents of the ACF's are available in the literature [16] and the field off CCF's vanish.

Orientational ACF components (see Sect. 2) were computed for the pump laser frequencies zero, 30, 300, 500, and 600 THz. From 30 to 600 THz applied laser frequency the Z component has a clearly different time dependence from those of the X and Y components, which evolve on closely similar lines. There is a variety of behaviour, markedly dependent on the pump laser frequency. It is interesting to note in Fig. 4 at 30.0 THz the presence of 0.033 ps oscillations, showing the influence

in the water molecule dynamics of a 30 THz pump laser. These 0.033 ps oscillations are superimposed on a clear, though weak, mirror image, pattern of orientational cross correlation in the frequency doubled optical Stark effect due to a 30 THz pump laser. The orientational CCF's are barely distinguishable from noise at 300, 500 and 600 THz. Note that the Fourier transform of the orientational ACF representing the axis ($\underset{\sim}{\varrho}_1$) of the permanent electric dipole moment in water is related to the dielectric loss spectrum [18] and is therefore observable experimentally.

Similarly, the Fourier transform of the time ACF of $\dot{\underset{\sim}{\varrho}}_1$ (the rotational velocity ACF) is related to the far infra red power absorption coefficient [18] and sequencies of rotational velocity ACF's nd CCF's were computed. At zero pump laser frequency the X component is clearly independent of the other two in its time evolution, whereas for applied laser frequencies from 30 to 600 THz, the Z component is the one that is independent. This echoes the same type of "anisotropy switch" seen in the rise transients. The details of the oscillations are clearly determined by the pump laser frequency, implying that the far infra red spectrum would also be determined by the characteristics of the pump laser. Very weak but real, oscillations appear at the inverse of the pump laser frequency superimposed on the X and Y components. The value 0.003 ps (inverse of 300 THz) nears the limit of our time resolution, which for these data is two time steps, or 0.001 ps, i.e. 1.0 fs. For this reason a run at 600 THz was repeated with a time step of 0.1 fs, with the result shown in Fig. 3. The accompanying rotational velocity CCF's of the data set display a variety of behaviour and are clearly distinguishable from noise, with the possible exception of the CCF at zero applied laser frequency. It is notable that the CCF's are sometimes in a "mirror image pattern", as at 30 THz, and sometimes positive at $t=0$ (300 and 500 THz), and sometimes negative at $t=0$ (600 THz). At 300, 500, and especially at 600 THz (time step of 0.5 fs), incompletely resolved oscillations appear at 0.0033, 0.002, and 0.0016 ps respectively on the principal structure of the component CCF's. Reducing the time step to 0.1 fs at 600 THz resolves the 0.0016 ps oscillation more clearly.

For both orientational and rotational velocity ACF's and CCF's it is clear that the complicated interaction of laser and ensemble dynamics (Brownian motion [18]) in the frequency doubled optical Stark effect results in the development of anisotropy, which can be measured through transient birefringence, dielectric or far infra red spectra. When dealing with the magnetic properties of ensembles it is useful to recall that the parity inversion (P) and time reversal (T) symmetries of the magnetic dipole moment are the same as those of angular momentum (P positive, T negative). One is in general proportional to the other through a scalar quantity, whose precise meaning is a matter of context. In NMR, for example, it is the nuclear gyromagnetic ratio, in ESR it is the electronic counterpart. It follows that the angular momentum time correlation tensor $\underset{\sim}{C}_1$ is also a magnetic dipole moment time correlation tensor. The sequence for $\underset{\sim}{C}_1$ corresponding to those for $\underset{\sim}{C}_2$ and $\underset{\sim}{C}_3$ (ACF's and CCF's more an "anisotropy switch" between the result for zero frequency pump laser and the other results, which range from 30 to 600 THz. The details of the time evolution of the components of $\underset{\sim}{C}_1$ depend on the applied laser frequency, and it is interesting to note that incompletely resolved oscillations at 0.0033, 0.002, and 0.0016 ps can be seen once more in these correlation functions, but this time in the Z component, and not in the X and Y components as for their rotational velocity counterparts. All components at all frequencies appear to oscillate about a zero $t\rightarrow\infty$ level, so that there is no magnetisation. This is in contrast to a parallel simulation [25] of the inverse Faraday effect [26] where magnetisation was observed as a non vanishing $t\rightarrow\infty$ component of the ACF of $\underset{\sim}{C}_1$ in the laser propagation axis. This shows clearly the difference between the optical Stark effect, and the optical Zeeman effect, which relies on the conjugate product of the pump laser [27] and the antisymmetric, or vectorial, part of the molecular polarisability [28, 29]. An interesting variety of CCF's of $\underset{\sim}{C}_1$ was found in terms of the XY and YX components, orthogonal to the Z propagation axis of the pump laser. The strongest cross correlation is that at 30 THz (Fig. 7), which is an order of magnitude greater than the others, computed at zero frequency, and at 300 to 600 THz. The latter are weak but nevertheless finite, and characteristic therefore of the frequency doubled optical Stark effect.

4. Discussion

In this paper we have carried out what appears to be the first FMD simulation of the Frequency doubled optical Stark effect, and have shown that even though the torque (15) is time dependent, second order rise transients, with what appear to be time independent final levels, develop in response to the applied pump laser. These cannot be analysed with Langevin Kielich functions [2], however, because the time average of the Hamiltonian (9) vanishes. (It was shown in the early days of FMD [9] that where Langevin functions and Langevin Kielich functions exist, the FMD results are in good agreement. This finding has been confirmed recently [30] in an FMD simulation of the optical Kerr effect, where the Hamiltonian and torque are time independent.) The existence of second and higher even order orientational rise transients has also been shown by FMD in a recent simulation of the inverse Faraday effect [25]. In both the inverse Faraday effect and in the frequency doubled optical Stark effect, the existence of transients signal that of transient birefringence. The latter is observable in principle by adaptations of contemporary optical Kerr effect apparatus with femtosecond time resolution [23].

In order to measure the effect of the torque (15) of the frequency doubled optical Stark effect on far infra red and dielectric spectra, an experimental compromise has to be forged between the need for short high intensity pump laser pulses, and the measurement time of a spectrum. Contemporary Fourier transform spectrometers can measure a far infra red spectrum in the millisecond to

with a medium intensity pump laser pulse. It appears entirely possible, with ingenuity, to devise a design for the experimental investigation of the effect of pump laser pulses on a far infra red spectrum thus bringing together two major fields of investigation: far infra red and nonlinear spectroscopy and optics. Interpretation of such spectra would rely, as in this paper, on FMD methods, which are applicable to any type of molecular dynamics source code in which a torque is computed in the forces loop. Such a procedure welds a point of contact between FMD and experimental data, the other point of contact, clearly, being femtosecond measurements of birefringence, or by Kramers Kronig transform, anisotropy in power absorption coefficient of a probe laser. The latter is implemented, as usual, in addition to pump laser pulses, and the two lasers are used to measure rise transients directly on a femtosecond time scale [23]. This type of methodology for the customary, frequency independent, optical Stark effect, is well developed experimentally [31–33], usually in the context of quantised optical Stark splitting in gases. This paper has shown that there is also a frequency doubled optical Stark effect, producing second order rise transients, birefringence and anisotropy in liquids as well as gases. Our treatment has necessarily been confined however to classical dynamics.

Finally, we note that the simulations have been performed with the equivalent of very intense lasers simply in order to isolate the existence of the effects reported in this paper from background noise. Experimentally, pump probe methods use a sub-picosecond pulse of intense laser radiation followed at an interval by a probe. These methods are used with efficient thermostats to remove any heating effects. The power of the pump laser pulse can reach the megawatt level, yet the liquid sample does not evaporate or heat because: 1) the pulse lasts for less than a picosecond: 2) the thermostats used experimentally are efficient dissipators of any heating effects. It is clear that the frequency doubled optical Stark type birefringence anticipated in this FMD simulation is a bi-axial birefringence, i.e. the refractive index in the pump laser's propagation axis, Z, becomes different from those in the orthogonal X and Y axes. Therefore the refractive index also becomes different in the Z axis from the field off value. This occurs at double the frequency of the pump laser, so that these two characteristic features isolate the effect. In general the refractive index is made up of a weighted combination of the second order orientational averages observed in the simulation (Fig. 2), and is also related to the measurable power absorption coefficient through the Kramers Kronig equations. The experiment can therefore proceed by measuring, at twice the pump laser frequency, the change in the power absorption coefficient produced in the sample by the pump laser with a probe laser appropriately timed, tuned and detected. The contemporary technology for this experiment is well established, the probe being timed to follow the pump at a convenient interval with optical delay lines, consisting of beam splitters and mirrors as in the sub-picosecond optical Kerr effect [23]. The latter is usually detected however by a change in the plane of polarisation of the probe. In the frequency doubled optical Stark effect, the probe need not be polarised.

Prof. Dr. George Wagnière and Prof. Dr. Stanisław Woźniak are thanked for many interesting discussions. Prof. Wagnière is thanked for an invitation to the University of Zürich and the Swiss NSF for funding this project.

References

1. Hanna, D.C., Yuratich, M.A., Cotter, D. (eds.): Nonlinear optics of free atoms and molecules. (Springer Series in Optical Sciences, Vol. 17) Berlin, Heidelberg, New York: Springer 1979
2. Kielich, S.: In: Davies, M. (Senior Reporter): Dielectric and related molecular processes, vol. 1. London: Chemical Society 1972
3. Kielich, S.: Nonlinear molecular optics. Moscow: Nauka 1981
4. O'Konski, C.T., Yoshioka, K., Orttung, W.H.: J. Chem. Phys. **63**, 1558 (1959)
5. Wagnière, G.: Phys. Rev. A**40**, 2437 (1989)
6. Barron, L.D.: Molecular light scattering and optical activity. Cambridge: Cambridge Univ. Press 1982
7. Woźniak, S., Wagnière, G., Zawodny, R.: Phys. Lett. A (in press)
8. Woźniak, S., Zawodny, R.: Phys. Lett. A**85**, 111 (1981)
9. Evans, M.W.: J. Chem. Phys. **76**, 5473, 5480 (1982); **77**, 4632 (1982); **78**, 925 (1983); **79**, 5403 (1983)
10. Evans, M.W., Coffey, W.T., Grigolini, P.: Molecular diffusion, chapters 1 and 2. New York: Wiley Interscience 1984; Moscow: MIR (1988)
11. Evans, M.W., Grigolini, P., Pastori, G., Prigogine, I., Rice, S.A. (eds.): Advances in chemical physics, vol. 62, chapter 5. New York: Wiley Interscience 1985
12. Evans, M.W., Lie, G.C., Clementi, E.: J. Chem. Phys. **87**, 6040 (1987)
13. Evans, M.W., Lie, G.C., Clementi, E.: Z. Phys. D – Atoms, Molecules and Clusters **7**, 397 (1988)
14. Evans, M.W.: In: Prigogine, I., Rice, S.A. (eds.): Advances in chemical physics, vol. 81. New York: Wiley Interscience (in press)
15. Evans, M.W.: J. Mol. Liq. **34**, 269 (1987)
16. Evans, M.W., Swamy, K.N., Refson, K., Lie, G.C., Clementi, E.: Phys. Rev. A**36**, 3935 (1988)
17. Evans, M.W., Lie, G.C., Clementi, E.: J. Chem. Phys. **88**, 5157 (1988)
18. Evans, M.W., Evans, G.J., Coffey, W.T., Grigolini, P.: Molecular dynamics, chapter 1. New York: Wiley Interscience 1982
19. Evans, M.W., Woźniak, S., Wagnière, G.H.: Physica B (in press)
20. Khanarian, G., Kent, L.: J. Chem. Soc. Faraday Trans. 2 **77**, 495 (1981)
21. Zeiss, G.D., Meath, W.J.: Mol. Phys. **30**, 161 (1975)
22. Jortner, J., Levine, R.D., Prigogine, I., Rice, S.A. (eds.): Advances in chemical physics, vol. 47. New York: Wiley Interscience 1981
23. Kalpouzos, C., McMorrow, D., Lotshaw, W.T., Kenney-Wallace, G.A.: Chem. Phys. Lett. **150**, 138 (1988)
24. Evans, M.W., Lie, G.C., Clementi, E.: Phys. Lett. A**130**, 289 (1988)
25. Evans, M.W., Woźniak, S., Wagnière, G.H.: Physica B (in press)
26. Pershan, P.S., Ziel, J.P. van der, Malmstrom, L.D.: Phys. Rev. A**143**, 574 (1966)
27. Evans, M.W.: Phys. Rev. Lett. **64**, 2909 (1990)
28. Evans, M.W.: Phys. Chem. **95**, 2256 (1991)
29. Evans, M.W.: Chem. Phys. **150**, 197 (1991)
30. Evans, M.W., Woźniak, S., Wagnière, G.H.: Physica B (in press)
31. Shen, Y.R.: The principles of non-linear optics. New York: Wiley 1984
32. Gray, H.R., Stroud, C.R.: Opt. Commun. **25**, 359 (1978)
33. Molander, W.A., Stroud, C.R. Jr., Yeazell, J.A.: J. Phys. 19, L461 (1986)